PCCP

Accepted Manuscript

ROYAL SOCIETY OF CHEMISTRY

www.rsc.org/pccp

Efficiency enhancement of cubic perovskite $BaSnO_3$ nanostructures based dye sensitized solar cells

N. Rajamanickam[a,b], P. Soundarrajan[b], Venkat K. Vendra[a], Jacek B. Jasinski[a], Mahendra K. Sunkara[a], and K. Ramachandran[b]

[a] Conn Center for Renewable Research and Department of Chemical Engineering, University of Louisville, Louisville, KY – 40292, USA.

[b] School of Physics, Madurai Kamaraj University, Madurai – 625021, TN, India.

* Corresponding author E-mail: nrajamku@gmail.com

*Tel. No: +91-0452-2458471 (352)

*Fax: +91-0452-2458471

Abstract

Cubic perovskite $BaSnO_3$ (BSO) is an important photoelectron transporting material due to its electronic structure that in competes with TiO_2 in dye-sensitized solar cells (DSCs). Separately, the BSO/$TiCl_4$ treatment and BSO/scattering layer photoelectrodes have been used in DSCs that effectively increase the photoexcited charge carriers collection resulting in superior photovoltaic performance. In the present work, the different $TiCl_4$ treatment time (1, 3 and 5 min), different scattering layer (tetragonal anatase TiO_2 and hexagonal wurtzite ZnO) and both are successfully used on BSO nanocuboids/nanoparticle morphological structure photoelectrodes and then systematically inspected their performance in DSCs. Under the optimized conditions, the power conversion efficiency (PCE) of 3.88% is obtained on BSO/$TiCl_4$ treatment photoanode. Furthermore, the BSO photoanode, made by scattering layer such as anatase TiO_2 and hexagonal ZnO i.e., BSO/anatase TiO_2 and BSO/hexagonal ZnO exhibited the PCE of 1.14% and 1.25% respectively. In the end, one of the highest PCE (5.68%) has been achieved using BSO/$TiCl_4$ treatment/TiO_2 scattering layer photoanode. Another photoelectrode such as BSO/$TiCl_4$ treatment/ZnO scattering layer exhibited the PCE of 4.28% that is also higher than the BSO/$TiCl_4$ treated and BSO/scattering layer photoanodes. Electron lifetime versus current density studies illustrate the stability of the BSO photoelectrode in DSCs. From the observed result, it is realized that the BSO is one of the most important future technological materials.

Keywords: Perovskites, $BaSnO_3$, nanocuboids, scattering layer, $TiCl_4$ treatment, dye-sensitized solar cells.

1. Introduction

The pioneer investigation of dye-sensitized solar cell (DSC) by O'Regan and Gratzel in the nineties has stimulated special attention among nanotechnologist owing to its affordable fabrication process and then it has been considered as a promising next-generation solar cell candidate according to its remarkable PCE.[1-3] Typically, the DSCs fabricated by injection of liquid electrolyte between sandwiched working (dye loaded large band-gap semiconductor) and counter (platinum) electrode. The overall performance of the fabricated device mainly depends on the following processes (i) amount of dye loading (ii) light scattering capacity (iii) photoinduced charge separation (iv) interfacial charge transfer and (v) recombination rate.[3-8] Hence it is realized that the superb physical and chemical properties of photoanode materials with expected particle size (or) morphological structures played a key role for controlling the above-mentioned points in DSCs. For achieving higher PCE, a numerous metal oxide semiconductor systems have been investigated.[9-11] Until now the wide-bandgap TiO_2 mesoporous morphological structure semiconductor is a most convincing photoanode material in DSC.[3, 12]

So far, the relevant investigations have mainly focused on either modifying the TiO_2 photoelectrode or choosing other components such as liquid electrolyte and/or dye molecules. Recently, one of the record PCE (~12%) has been achieved by using pophyrin-sensitized meso-porous TiO_2 photoanode and cobalt redox electrolyte solution.[1] On the other hand, another metal oxides such as ZnO,[13-16] SnO_2,[17, 18] and Nb_2O_5[19] have been investigated during the search of alternatives, but none of them could exhibited comparable device performance. These report opened a new door for searching ternary metal oxide semiconductors including Zn_2SnO_4, $ZnTiO_3$, $SrTiO_3$,

etc., The reason may be due to their ionization potential and electron affinity can be easily modified via controlling the bond (ionic (or) covalent) energy of valence electrons with respect to altering their atomic composition during synthetic strategy.[2, 20] Hence, few researchers have been investigated ternary metal oxides as photoanodes in DSCs where an efficiency of < 6% achieved in Zn_2SnO_4.[21-23]

Recently, perovskite $BaSnO_3$ material has exhibited their excellent contribution in various applications including high-temperature superconductivity,[24, 25] colossal magneto résistance,[26, 27] electro chemical activity,[28] ferromagnetism,[29, 30] ferroelectricity,[31-33] sensors and multiferroics.[34, 35] The generation of photoelectrons can be easily controlled by tuning of atomic composition or impurity adding into the Ba or Sn site.[3, 20, 36, 37] Different thickness of BSO layer photoelectrodes and various dye molecules have been successfully used in DSCs and achieved reasonable PCE.[2, 20, 38, 39]

Electron transporting material in DSCs has been transmitted large portion of visible light energy through it. Therefore that exhibited poor scattering effect with respect to its wide bandgap and small particle size (20-30 nm).[40] One of the possible ways was introducing an optical scattering layer on photoelectrode which increases the life time of incident light. This new route has been recently employed to explore their impact on working electrode and investigated their device performance.[41, 42] Therefore, the 4-5 μm thick layer film, consist of large size nanoparticles (or) nanopores coated on the top of the electron-transporting material, has increased the PCE,[43, 44] The particle size of 400 nm TiO_2 layer also act as a light scattering layer which effectively increased the incident light energy path, result in improving the photocurrent density.[45] Furthermore, the spherical shaped TiO_2 nanoparticles have been also used as a scattering layer for improving PCE.[46] In addition, the hierarchal ZnO parallelopipeds and cubic CeO_2

nanostructures have been introduced as a scattering layer.[3, 47] Hence it is empirically realized that the BSO photoelectrode based DSCs is still in infancy and remain exist many opportunities.

Therefore, the main aim of the present work is increasing the PCE of DSCs using modified BSO photoelectrodes. Initially, the BSO nanocuboids/nanoparticles morphological structure has been synthesized using co-precipitation method. Subsequently, the BSO coated on the FTO substrate and used as photoanode in DSCs. The $TiCl_4$ treatment, scattering layer (TiO_2 and ZnO) and both are used on BSO coated FTO substrate and exploited as a photoelectrode in DSCs. It investigated that the $TiCl_4$ treatment/ scattering layer used on BSO photoelectrode is concurrently increased the life time of incident light and charge collection during device performance resulting in higher PCE. Because of newness of this photoelectrode, the structural and morphological properties of synthesized BSO, BSO/$TiCl_4$ treatment, BSO/$TiCl_4$ treatment/scattering layer photoanodes and their performance in DSCs have been reported here.

2. Experimental Section

2.1. Synthesis of BSO nanostructures

Nanocrystalline BSO powder were prepared via modified oxalate co-precipitation method.[48] In briefly, 0.1 M of commercially purchased $BaCl_2$ and $SnCl_2$ (high purity (99%)) were separately dissolved in double distilled water and then continuously stirred for 30 min. These separate solutions were slowly mixed together under gentle stirring. Additionally, 0.2 M of aqueous oxalic acid solution was mixed into the above stock solution. The white oxalate precipitate was initially formed and then stirred continued for another 3 hours. Finally, the reactant solution was washed several time

using distilled water and then dried at 110 ^{o}C for overnight. The obtained BSO was annealed at 900 ^{o}C for 3 hours using muffle furnace.

2.2. Preparation of BSO electrode

BSO nanocrystalline films were prepared on FTO covered glass substrates from a homemade BSO paste via a doctor-blade method.[49, 50] First, the synthesized BSO was converted into fine paste by grinding 0.1 g of BSO with distilled water. Then 0.02 ml of acetyl acetone was slowly added. Furthermore, this viscous paste was pestle for 10 min. Finally, 0.34 ml of distilled water and 20 µl of triton-X 100 were gradually mixed for getting uniform BSO paste. The resultant paste was coated on FTO substrate by using doctor blade technique with a cell area of 1 cm^2. The coated film lifted to dry in ambient conditions and then annealed at 500 °C for 30 min in air.

2.3. Preparation of BSO/$TiCl_4$ treatment electrodes

For the $TiCl_4$ treatment, the annealed BSO films were drowned into aqueous solution of 0.05 M $TiCl_4$ at 50 °C. Different time (1, 3, and 5 min) $TiCl_4$ treated electrodes were prepared and subsequently sintered using muffle furnace at 500 °C for 30 min.

2.4. Preparation of BSO/Scattering layer (BSO/TiO_2 and BSO/ZnO) electrodes

TiO_2 nanocrystalline paste was purchased from the Dyesol, Australia. The ZnO nanoparticles were prepared in our laboratory by using Plasma-enhanced chemical vapor deposition (PECVD) method. Following this process, the ZnO nanoparticles were converted into fine paste by grinding 0.1 g of ZnO nanoparticles with distilled water and 4 µl acetyl acetone using mortar. After that the paste was pestle for 10 min. Furthermore, 0.135 ml of distilled water and 2 µl triton-X 100 were slowly added into above paste with continuous mixing result in uniform ZnO paste. The purchased TiO_2 paste and prepared ZnO paste were coated on BSO covered FTO substrate via doctor

blade technique. These electrodes (BSO/TiO_2 scattering layer and BSO/ZnO scattering layer) were again sintered at 500 ºC for 30 min in air.

2.5. Preparation of BSO/$TiCl_4$ treatment/scattering layer electrodes

After fabrication of BSO/$TiCl_4$ treatment and BSO/scattering layer electrodes, our research team carefully fabricated novel BSO/$TiCl_4$ treatment/scattering layer electrode by directly coating TiO_2 and ZnO past on BSO/(1, 3 and 5 min) $TiCl_4$ treated FTO substrates via doctor blade technique.

2.6. Dye preparation

For dye absorption, the BSO, BSO/$TiCl_4$ treatment, BSO/scattering layer (BSO/TiO_2 and BSO/ZnO) and BSO/$TiCl_4$ treatment/scattering layer electrodes were drowned in an ethanol solution for 1 h at room temperature that contains 0.5 mM of Ru complex dye (N719) at room temperature. The soaking time of the BSO film in the dye molecules is much shorter than the conventional materials (TiO_2). This may be due to the fast dye adsorption kinetics of the BSO surface. Following this process, the prepared electrodes were rinsed with a mild stream of absolute ethanol to remove the physically adsorbed dye molecules.

2.7. DSC assembly

The sandwich-type DSCs were assembled using dye-adsorbed BSO photo electrode and platinum-coated counter electrode. In briefly, the counter electrode was prepared by a drop of 5 mM chloroplatinic acid hexahydrate (H_2PtCl_6) dissolved in isopropyl alcohol and spreading on separate FTO substrate and then sintered at 450 °C for 15 min in air. The prepared photoelectrode sandwiched with counter electrode by using parafilm spacer to avoid short-circuit between working and counter electrode. Consequently, one drop of iodide-based liquid electrolyte (EL-HPE; Dyesol, Australia) was carefully injected in between the electrodes. Two binder clips were

clamped to maintain the mechanical grip for avoiding disturbance during cell operation. Here the 1 cm^2 active area of the dye-coated BSO film was used as photoelectrodes. The schematic diagram of the fabrication device is shown in Fig. 5.

2.8. Material characterizations

The crystallinity and phase purity of the BSO material and fabricated photoelectrodes were characterized using X-ray diffractometer (XRD) (PANalytical X'Pert Pro (with Cu-Kα radiation)). The synthesized BSO was excited using a 488 nm Ar^+ laser line through LabRam HR800 micro-Raman instrument, and its backscattering mode was recorded in the wavenumber range of 100-800 cm^{-1}. The shape, size and lattice dimension of the BSO material were analysed using transmission electron microscope (TEM) and high-resolution TEM (HRTEM) (FEI Tecnai G2). Additionally, the HRTEM image captured for crystalline TiO_2 and ZnO crystalline samples. The top view of synthesized nanocrystalline BSO powder, top and cross-section view of the BSO/scattering layer and cross-section view of BSO/1 min $TiCl_4$ treatment/scattering layer photoelectrodes surface morphologies were captured using a scanning electron microscope (SEM) (Tescan VEGA3) and field emission SEM (FEI NOVA nano SEM 600) respectively.

2.9. Device testing

The prepared DSCs were illuminated using a xenon lamp of 150W solar simulator (New port model 96000) equipped with an Air Mass 1.5 filler. Intensity of incident light was adjusted to 100 mW cm^{-2} using a silicon power meter (Thorlabs S120UV). The charge carriers have been generated by a short time of incident light and the life time of the carrier density with time is measured.

3. Results and Discussion

3.1. Characterization of synthesized BSO material

Until now, the XRD characterization technique separately gives the progress card to prepared materials are eligible for making electronic and optoelectronic devices. Hence, our synthesized nanocrystalline BSO was carefully examined to XRD analysis. In order to confirm the purity of the phase structure, a Rietveld refinement carried out for XRD data of the BSO sample (2θ range 20 - 80º) and the observed result is shown in Fig. 1(a). According to ICDD No 15-0780, the observed lattice planes exhibited the cubic perovskite structure without any ambiguity, and having a lattice constant of 4.113 Å. It can be seen that most of the cubic perovskite BSO structure is constructed by the (110) crystallographic plane owing to its higher surface energy under synthetic strategy. The average crystallite size is calculated via well-known Scherrer equation using full width at half maximum (FWHM) of preferentially oriented crystallographic peak and it was found to be ~23 nm. Additionally, the strain (δ) and dislocation density (DD) values are calculated and presented in Table 1 (formula is given in SI). From the final refinement convergence R-pattern, the weighted profile R-pattern and S values are achieved and tabulated (Table 1). The obtained cubic phase unit cell of BSO from the Rietveld refinement is shown in Fig. 1(b) and it has space group $Pm\bar{3}m$. The micro-Raman spectrum of BSO is shown in Fig. S1. It is strongly supported the XRD result.

Following XRD and μ-Raman analyses, we accurately determine the shape, lattice dimension and crystal structure of the BSO material using TEM, HRTEM and SAED pattern respectively. The captured images (TEM, HRTEM and SAED pattern) are shown in Fig. 2. For the first time, it is observed that the BSO nanocrystalline powder exhibiting the nanocuboids/nanoparticles morphological structure. The low magnification TEM images (Fig. 2(a-d)) indicate the length and breadth range of nanocuboids are ~123 – 250 nm and ~118-236 nm respectively. The measured

interplanar spacing value from Fig. 2(e) is 1.923 Å and 2.885Å, which corresponding to the (200) and (110) crystallographic planes of the cubic BSO. The HRTEM image of the nanocuboid particles shows no stacking faults and dislocations that indicate the high purity and good crystallinity of nanocuboids shaped BSO. The selected area electron diffraction (SAED) pattern of BSO sample is shown in Fig. 2(f). The electron diffraction rings are assigned to the (110), (111), (200), (201), (220), (310), and (320) diffraction planes of BSO cubic phase. More importantly, the SAED patterns rings are in good agreement with the XRD and μ-Raman results. HRTEM images of the purchased TiO_2 and synthesized ZnO powders are shown in Fig. S2. From these images, the tetragonal anatase TiO_2 and hexagonal wurtzite ZnO crystal structures have been clearly confirmed.

In order to identify the presence of atomic level elements, the BSO sample examined to energy dispersive spectroscopic analysis (EDX). The obtained EDS spectrum is shown in Fig. 4(e). Here, we can see only the Ba, Sn and O atoms that are clearly indicated the prepared BSO material has high purity. Furthermore, the purity of TiO_2 and ZnO samples has checked by the EDX analysis and obtained spectrum is shown in Fig. S3 (a) and (b) respectively.

3.2. Characterization of fabricated BSO photoelectrodes

In BSO/ (1 and 3 min) $TiCl_4$ treatment electrodes, the extra diffraction peak is not clearly observed. Hence, the XRD patterns of the BSO/5 min $TiCl_4$ treatment based electrodes are only provided here. Fig. S4 shows the XRD pattern of BSO, BSO/5 min $TiCl_4$ treatment and BSO/5 min $TiCl_4$ treatment/ (ZnO and TiO_2) scattering layer electrode samples. Importantly, Rietveld refinement carried out for BSO/5 min $TiCl_4$ treatment and BSO/5 min $TiCl_4$ treatment/ (ZnO, TiO_2) scattering layer electrode samples and shown in Fig. 3. Due to $TiCl_4$ treatment on BSO, a new diffraction peak

erupted at 2θ value 25.33º, which attributed to the (101) crystallographic plane of anatase TiO_2. Compare with previous work, it indicates the shell-like anatase TiO_2 formed on the core BSO nanostructures.[13] In BSO/5 min $TiCl_4$ treatment/TiO_2 scattering layer electrode, the intensity of the anatase TiO_2 peak is increased and also few new peaks emerged on there. The ZnO scattering layer on BSO electrode has also exhibited few new diffraction peaks around 2θ value 31.78º, 34.43º and 36.26º which corresponding to the hexagonal wurtzite ZnO structure.

Fig. 4(a) shows the top view FESEM image of cubic perovskite structure of BSO nanocuboids/nanoparticles covered FTO substrate. This image clearly shows the nanocuboids surface morphological structure of BSO. The sizes of the cuboids are in the range of ~114- 310 nm and well-agreement with the TEM analysis. The top and cross-section view of the TiO_2 and ZnO scattering layer on perovskite BSO film are shown in Fig. 4(b, f) and (e, g) respectively. The particle size of the TiO_2 and ZnO scattering layer is in the range of ~80-230 nm and 300-400 nm respectively. The cross-section view of novel photoanodes such as BSO/1 min $TiCl_4$ treatment/TiO_2 scattering layer and BSO/1 min $TiCl_4$ treatment/ZnO scattering layer electrodes is shown in Fig. 4(d) and (h) respectively. Thickness of the bare BSO electrode is ~5 μm. Further, the measured thicknesses value of BSO/$TiCl_4$ treatment/TiO_2 scattering layer and BSO/$TiCl_4$ treatment/ ZnO scattering layer electrodes are ~8 μm and ~12 μm, respectively. With respect to increasing $TiCl_4$ treatment time on BSO, the thickness of the electrodes is slightly increased (~25-40 nm). This new type of photoanodes enhances the PCE by increasing both efficient charge collections and lifetime of incident light under reducing recombination event.

3.3. Photovoltaic discussion

The percentage of dye loading on the photoelectrode is strongly affecting its photocurrent density. Hence the amount of dye loading on BSO photoelectrode is optimized with respect to immersion time into dye molecules. Here, the optimized dye loading time is about 1 h. Compare with traditional TiO_2, the optimized dye loading time is very low in BSO material. Fig. 5 illustrates the schematic diagram of fabricated DSC that includes perovskite nanocrystalline wide-band gap BSO material on FTO substrate. When light energy passed through fabricated DSCs that generate the voltage across it. As a consequence, the photoelectrons are generated and build a path in which they would be travelling to surface of the working electrode. This process is majorly dependent on the following physico-chemical reactions.

$D + h\upsilon \rightarrow D^*$	Absorption or Excitation	(1)
$D^* \rightarrow D^+ + e^-(CB)$	Electron injection	(2)
$2D^+ + 3I^- \rightarrow 2D + I_3^-$	Regeneration	(3)
$I_3^- + 2e^-\ (Pt) \rightarrow 3I$	Reduction	(4)
$D^+ + e^-(CB) \rightarrow D$	Recombination	(5)
$I_3^- + 2e^-(CB) \rightarrow 3I^-$	Recaption	(6)
$D^* + D^+ \rightarrow D$	Relaxation	(7)

where D and D* are HOMO and LUMO level of dye molecules (Ru) and I is related to redox mediator. The first four reactions produce a clear route for excited electrons to make travel in the desired direction and fulfill the circuit. Consequently, another three reactions (5 to 7) referred as a dark reaction because it involved to decreases the output value of device performance. The expected chemical reaction under light irradiation associated with the potential difference between fermi level of the BSO and redox iodide electrolyte. Here the shift in fermi level is stimulated by accumulation of excited electrons in the conduction band edge of large band-gap BSO semiconductor.

Therefore, the adjustment of band-bending can be caused by structure of photoelectrodes that supported to generating the hot electrons from the incident solar photons without suffering any permanent chemical transformation. Different Ti source materials post-treatment carried out for adjusting band-bends result in increasing of PCE.[51] Furthermore, owing to the scarcity of the number of solar photons staying time in the device, the scattering layer have been effectively used for increasing PCE.[47] It has studied that the submicron particle size of TiO_2 and ZrO_2, and different ZnO nanostructures including nanowire, hierarchical structures, mesoporous spheres served as scattering layer were also used.[50] Additionally, the mirror like scattering layer has been recently reported for increasing life time of incident light.[3, 52] When compared with other shape and structures, the reflectance distance is high in the spherical like nanoparticles. Further, it gives a short pathway to reflective light and then easily reached the dye molecule on the surface of BSO. Subsequently, the reflective light flux is increased over the dye anchored surface of BSO.Therefore it is realized that the over-layer on the nano crystalline BSO photoanode system will encourage the light scattering in DSCs especially in the red energy portion of the solar spectrum. The position of the energy levels interface between BSO/dye/electrolyte is fundamentally important for the function of DSCs as shown in Fig. 6(a) and (b). Hence, the interface chemistry played an important role for determining the conduction band edge and Fermi level edge alignment in the devices.

The dye molecules absorbed visible light and excited from highest occupied molecular orbital (HOMO) to lowest unoccupied molecular (LUMO) level. Therefore that generates the photoelectrons according to equation 1. The photoelectrons transport behaviour from the CBE of the BSO to surface of working electrode is significantly

dependent on its band-alignment which is presumably controlled by its physic-chemical and mechanical properties.

3.4. Photovoltaic performance

The BSO/dye, BSO/$TiCl_4$ treatment/dye, BSO/TiO_2 scattering layer/dye and BSO/$TiCl_4$ treatment/ scattering layer/dye photoanodes based devices are shown in Fig. 6(c, d, e and f) respectively. The TiO_2 and ZnO have chosen as scattering layers because of its energy level ideal with dye molecules. Importantly, the valence band edge of TiO_2 and ZnO are located near the band edges of perovskite metal oxide.[53] Additionally, the back-electron transfer from BSO material to the oxidized species (I_3^-) of electrolyte is very complicated process which leads to increases lifetime of charge carriers in the working electrode. Hence the expected energy level arrangement tries to receive high voltage with minimum loss that easily generates the charge separation between the absorber and selective contacts. A schematic diagram of light scattering process of TiO_2 and ZnO scattering layer on BSO photoanode is shown in Fig. 7(a) and (b) respectively.

The typical photocurrent density-voltage (J−V) curves for the BSO, BSO/$TiCl_4$ treatment, BSO/scattering layer (TiO_2 and ZnO) and BSO/$TiCl_4$ treatment/scattering layer photoelectrodes measured under simulated solar illumination (AM 1.5G, 100 mW cm^{-2}) are shown in Fig. 8 and 9. Fig. 8 shows the J-V curves of BSO, BSO/$TiCl_4$ treatment and BSO/$TiCl_4$ treatment/TiO_2 scattering layer electrodes based DSCs devices. The photocurrent density of BSO electrode based DSC is 1.74 mA cm^{-2}. Different $TiCl_4$ treatment time (1, 3 and 5 min) has selected in order to identify the optimum condition for increasing PCE. Initially, the J_{sc} rapidly increased to 13.08 mA cm^{-2} at 1 min $TiCl_4$ treatment time and then they gradually decreased with respect to increasing $TiCl_4$ treatment time up to 5 min. The obtained higher J_{sc} value indicates

the large band gap BSO material have efficient charge collection capacity under slight modification of surface characteristics. The chemisorption of dye molecules on TiO is mainly dependent on the presence of OH species. In our work it is under investigation. Hence the lower dye adsorption may be due to reduce the presence of OH species with respect to increasing $TiCl_4$ treatment time. The $TiCl_4$ treatment on ZnO and TiO_2 photoelectrode is tried to shift the CBE potential to negative values result in increasing V_{oc}.[13] Here V_{oc} value is slightly decreased (~0.15 V) with respect to $TiCl_4$ treatment time. For this reason, the J_{sc} and V_{oc} values are gradually decreased with 3 and 5 min $TiCl_4$ treated BSO photoanode. Similar result is also observed from the BSO/scattering layer (ZnO and TiO_2) photoelectrode based DSCs. Finally, the maximum photocurrent density (16.67 mA cm^{-2}) is obtained in BSO/1 min $TiCl_4$ treatment/TiO_2 scattering layer photoanode. The electronic structure at the interface (BSO/$TiCl_4$ treatment/scattering layer) should be engineered to assuage detrimental effects such as surface recombination and fermi-level pinning which decisively helps to improve the J_{SC} under fast electron transport. Further, the photocurrent density of BSO/3 min $TiCl_4$ treatment/TiO_2 scattering layer and BSO/3 min $TiCl_4$ treatment/ZnO scattering layer photoanode is 14.19 and 11.13 mA cm^{-2} respectively. However, 3 and 5 min $TiCl_4$ treated BSO photoelectrodes have superior light scattering ability, but these Jsc value is gradually decreased. This may be due to the change in band-bending alignment with respect to $TiCl_4$ treatment time. It is also reported that the photo voltage (V_{oc}) declines gradually with increasing of $TiCl_4$ treatment time. The augmentation of numerous short BSO and TiO_2 branches provides additional charge recombination sites resulting in higher recombination rate.[54]

The resultant observed photovoltaic parameters such as $V_{oc,}$ J_{sc}, FF and efficiency are summarized in Table 2. The observed highest PCE (5.68%) in BSO/$TiCl_4$

treatment/TiO_2 scattering layer is 8 fold increased (155%) as compare to efficiency of bare BSO photoanode. The BSO/5 min $TiCl_4$ treatment/TiO_2 scattering layer yields an overall efficiency of 3.27% however it is higher than the bare BSO. This observation clearly tell us $TiCl_4$ treatment time determine the light harvestment and recombination rate according to fast electron injection from the surface of BSO photoanode and percentage of dye loading.

The photovoltaic performances of BSO/$TiCl_4$ treatment/ZnO scattering layer photoelectrode based DSCs devices are shown in Fig. 9. The photovoltaic parameters are presented in Table 2. The BSO/ZnO scattering layer photoanode based DSCs device has exhibited the photocurrent density of 2.6 mA cm^{-2}. The BSO/1 min $TiCl_4$ treatment/ZnO scattering layer photoanode has also exhibited the maximum J_{sc} and the observed value is 10.02 mA cm^{-2}. The J_{sc} value is decreased with increasing of $TiCl_4$ treatment time. At 5 min $TiCl_4$ treatment time, the obtained J_{sc} value is 7.53 mA cm^{-2}. Further, it is observed that the V_{oc} is decreased from 0.837 to 0.647 V with respect to increasing $TiCl_4$ treatment time. The BSO/ZnO scattering layer electrode increases the efficiency than the bare BSO photoanode. Finally, 1 min $TiCl_4$ treatment/ZnO scattering layer on BSO photoanode has exhibited the higher efficiency (4.28%).Both scattering layers (ZnO and TiO_2) electrodes have exhibited the similar characteristic of V_{oc} and J_{sc}. Fig. 10 reveals the schematic diagram of bare BSO, BSO/$TiCl_4$ treatment and BSO/$TiCl_4$ treatment/scattering layer electrodes based DSCs and achieved maximum PCE is highlighted. Compare with BSO/1 min $TiCl_4$ treatment/TiO_2 scattering layer, the BSO/$TiCl_4$ treatment/scattering layer electrodes based DSCs exhibited lower PCE values. It is well known that the specific surface area of the material is directly proportional to the particle size. Therefore, the amount of dye loading is decreased in the ZnO scattering layer electrodes result in decreasing of PCE.

3.5. Electron lifetime in BSO photoelectrodes

The photoexcited electron lifetime (τ) is strongly associated with the recombination event in the DSCs.[55] In order to understand the influence of $TiCl_4$ treatment, scattering layer and both on the BSO photoelectrode, the electron lifetime vs current density curve for BSO/$TiCl_4$ treatment/TiO_2 scattering layer is plotted and is shown in Fig. 11(a). All fabricated DSCs have exhibited higher τ value with good stability. In 3 and 5 min $TiCl_4$ treatment with/without scattering layer photoelectrodes, the τ is slightly decreased which may be due to the higher recombination event. Furthermore, the plotted electron lifetime vs current density curve for BSO/$TiCl_4$ treatment/ZnO scattering layer electrodes curve is shown in Fig. 11(b). The electron lifetime of the BSO based DSCs is increased after the $TiCl_4$ treatment. The acceleration of photoelectrons by the $TiCl_4$ treatment and scattering layer can be attributed to few important factors. Hence the photo voltage value decreases with respect to increasing $TiCl_4$ treatment time. (i) At higher $TiCl_4$ treatment time the uncouple nanoparticles are altering the fermi level position that also limiting the charge carrier transport over the surface of the BSO nanostructures. (ii) Interface formed between BSO and TiO_2 nanoparticles (via scattering layer) that can be participating in the charge carrier transport phenomena. It was noticed that the formation of TiO_2 shell layer over the surfaces of BSO nanoparticles prevent the reaction of injected photoelectrons with the oxidized species (I_3^-) in the electrolyte according to physically separating them.[2] The higher conduction band edge position of TiO_2 than the BSO repulses the electrons toward the BSO side due to the energy level difference (Fig. 6). Therefore, the electron recombination rate is increased at BSO/5 min $TiCl_4$ treatment photoelectrodes. Compare with BSO/$TiCl_4$ treatment/ZnO scattering layer electrode, the fermi level position variation is very low in BSO/$TiCl_4$ treatment/TiO_2 scattering

layer electrode. Therefore the BSO/$TiCl_4$ treatment/TiO_2 scattering layer electrode has exhibited one of the highest PCE.

4. Conclusions

Initially, we have assembled the bare cubic perovskite BSO nanocuboids/nanoparticles morphological structure photoelectrode based DSCs that exhibited the PCE of 0.71%. Separately, two scattering layers (TiO_2 and ZnO) and $TiCl_4$ treatment (1, 3 and 5min) are carried out on BSO nanocuboids/nanoparticles and used as photoelectrodes in DSCs. The PCE of 1.14, 1.25 and 3.88% is observed for BSO/TiO_2 scattering layer and BSO/ZnO scattering layer and BSO/1 min $TiCl_4$ treatment photoanodes respectively. Finally, a novel BSO/$TiCl_4$ treatment/scattering layer photoelectrode has been successfully fabricated by our research team. For achieving maximum PCE, we planned to optimize the different time $TiCl_4$ treated photoanodes. Consider this point, 1, 3 and 5 min $TiCl_4$ treated BSO photoanode have been tested and the obtained PCE value is 3.88, 1.78 and 1.61% respectively. The aim of present work has been successfully satisfied by achieving one of the highest PCE value. The obtained highest PCE is 5.68% on BSO/1 min $TiCl_4$ treatment/TiO_2 scattering layer photoanode. In ZnO scattering layer based BSO photoelectrodes, the maximum PCE of 4.28% is obtained on BSO/1 min $TiCl_4$ treatment/ZnO scattering layer photoanode.

Acknowledgements

One of the authors NR (N. Rajamanickam) acknowledges DST-IUSSTF BASE Research Fellowship. The author KR (K. Ramachandran) acknowledges CSIR, New Delhi, for the financial support given in the form of Emeritus fellowship. The authors would like to thank Conn center for renewable research, University of Louisville, Louisville, USA.

Electronic Supplementary Information (ESI) available: See DOI: 10.1039/b000000x/

References

1. A. Yella, H.-W. Lee, H. N. Tsao, C. Yi, A. K. Chandiran, M. K. Nazeeruddin, E. W.-G. Diau, C.-Y. Yeh, S. M. Zakeeruddin and M. Grätzel, *Science*, 2011, **334**, 629-634.
2. S. S. Shin, J. S. Kim, J. H. Suk, K. D. Lee, D. W. Kim, J. H. Park, I. S. Cho, K. S. Hong and J. Y. Kim, *ACS Nano*, 2013, **7**, 1027-1035.
3. H. Yu, Y. Bai, X. Zong, F. Tang, G. Q. Max Lu and L. Wang, *Chem. Commun.*, 2012, **48**, 7386-7388.
4. F. Sauvage, J.-D. Decoppet, M. Zhang, S. M. Zakeeruddin, P. Comte, M. Nazeeruddin, P. Wang and M. Grätzel, *J. Am. Chem. Soc.*, 2011, **133**, 9304-9310.
5. P. Tiwana, P. Docampo, M. B. Johnston, H. J. Snaith and L. M. Herz, *ACS Nano*, 2011, **5**, 5158-5166.
6. F. Huang, D. Chen, X. L. Zhang, R. A. Caruso and Y. B. Cheng, *Adv. Funct. Mater.*, 2010, **20**, 1301-1305.
7. J.-Y. Liao, B.-X. Lei, D.-B. Kuang and C.-Y. Su, *Energ. Environ. Sci.*, 2011, **4**, 4079-4085.
8. K. Zhu, N. R. Neale, A. Miedaner and A. J. Frank, *Nano Lett.*, 2007, **7**, 69-74.
9. M. Quintana, T. Edvinsson, A. Hagfeldt and G. Boschloo, *The Journal of Physical Chemistry C*, 2007, **111**, 1035-1041.
10. K. S. Leschkies, R. Divakar, J. Basu, E. Enache-Pommer, J. E. Boercker, C. B. Carter, U. R. Kortshagen, D. J. Norris and E. S. Aydil, *Nano Lett.*, 2007, **7**, 1793-1798.
11. A. Kitiyanan and S. Yoshikawa, *Mater. Lett.*, 2005, **59**, 4038-4040.
12. M. A. Greeny, K. Emery, Y. Hishikawa and W. Warta, *Prog. Photovoltaics*, 2011, **19**, 84-92.
13. N. Sakai, T. Miyasaka and T. N. Murakami, *J. Phys. Chem. C*, 2013, **117**, 10949-10956.
14. A. Sacco, A. Lamberti, R. Gazia, S. Bianco, D. Manfredi, N. Shahzad, F. Cappelluti, S. Ma and E. Tresso, *Phys. Chem. Chem. Phys.*, 2012, **14**, 16203-16208.
15. N. Memarian, I. Concina, A. Braga, S. M. Rozati, A. Vomiero and G. Sberveglieri, *Angew. Chem.*, 2011, **123**, 12529-12533.
16. W.-C. Chang, C.-H. Lee, W.-C. Yu and C.-M. Lin, *Nanoscale Res. Lett*, 2012, **7**, 1-10.
17. Q. Wali, A. Fakharuddin, I. Ahmed, M. H. Ab Rahim, J. Ismail and R. Jose, *Journal of Materials Chemistry A*, 2014, **2**, 17427-17434.
18. A. Birkel, Y.-G. Lee, D. Koll, X. Van Meerbeek, S. Frank, M. J. Choi, Y. S. Kang, K. Char and W. Tremel, *Energ. Environ. Sci.*, 2012, **5**, 5392-5400.
19. R. Abdul Rani, A. S. Zoolfakar, J. Subbiah, J. Z. Ou and K. Kalantar-zadeh, *Electrochem. Commun.*, 2014, **40**, 20-23.
20. D. W. Kim, S. S. Shin, S. Lee, I. S. Cho, D. H. Kim, C. W. Lee, H. S. Jung and K. S. Hong, *ChemSusChem*, 2013, **6**, 449-454.
21. S. S. Shin, D. W. Kim, D. Hwang, J. H. Suk, L. S. Oh, B. S. Han, D. H. Kim, J. S. Kim, D. Kim and J. Y. Kim, *ChemSusChem*, 2014, **7**, 501-509.
22. J. Chen, L. Lu and W. Wang, *J. Phys. Chem. C*, 2012, **116**, 10841-10847.
23. B. Tan, E. Toman, Y. Li and Y. Wu, *J. Am. Chem. Soc.*, 2007, **129**, 4162-4163.
24. R. Cava, B. Batlogg, J. J. Krajewski, R. Farrow, L. Rupp, A. White, K. Short, W. Peck and T. Kometani, *Nature*, 1988, **332**, 814-816.
25. P. A. Lee, N. Nagaosa and X.-G. Wen, *Rev. Mod. Phys.*, 2006, **78**, 17.

26. W. Eerenstein, N. Mathur and J. Scott, *nature*, 2006, **442**, 759-765.
27. Y. Tokura, *Rep. Prog. Phys.*, 2006, **69**, 797.
28. Z. Xie, H. Zhao, Z. Du, T. Chen, N. Chen, X. Liu and S. J. Skinner, *J. Phys. Chem. C*, 2012, **116**, 9734-9743.
29. K. Balamurugan, N. Harish Kumar, B. Ramachandran, M. Ramachandra Rao, J. Arout Chelvane and P. Santhosh, *Solid State Commun.*, 2009, **149**, 884-887.
30. K. James, A. Aravind and M. Jayaraj, *Appl. Surf. Sci.*, 2013, **282**, 121-125.
31. M. K. Lee, T. K. Nath, C.-B. Eom, M. C. Smoak and F. Tsui, *Appl. Phys. Lett.*, 2000, **77**, 3547-3549.
32. A. Kumar, B. Singh, R. Choudhary and A. K. Thakur, *Mater. Lett.*, 2005, **59**, 1880-1888.
33. C. Shan, T. Huang, J. Zhang, M. Han, Y. Li, Z. Hu and J. Chu, *J. Phys. Chem. C*, 2014, **118**, 6994-7001.
34. G. Schileo, A. Feteira, I. M. Reaney, P. Postolache, L. Mitoseriu and K. Reichmann, *Int. J. Appl. Ceram. Technol.*, 2014, **11**, 457-467.
35. M. Bernardo, T. Jardiel, M. Peiteado, F. Mompean, M. Garcia-Hernandez, M. Garcia, M. Villegas and A. Caballero, *Chem. Mater.*, 2013, **25**, 1533-1541.
36. H. Mizoguchi, P. M. Woodward, C.-H. Park and D. A. Keszler, *J. Am. Chem. Soc.*, 2004, **126**, 9796-9800.
37. P. H. Borse, U. A. Joshi, S. M. Ji, J. S. Jang, J. S. Lee, E. D. Jeong and H. G. Kim, *Appl. Phys. Lett.*, 2007, **90**, 034103-034103-034103.
38. Y. Zhang, H. Zhang, Y. Wang and W. Zhang, *J. Phys. Chem. C*, 2008, **112**, 8553-8557.
39. F.-a. Guo, G. Li and W. Zhang, *Int. J. Photoenerg.*, 2010, **2010**.
40. Y.-C. Park, Y.-J. Chang, B.-G. Kum, E.-H. Kong, J. Y. Son, Y. S. Kwon, T. Park and H. M. Jang, *J. Mater. Chem.*, 2011, **21**, 9582-9586.
41. D. Chen, F. Huang, Y. B. Cheng and R. A. Caruso, *Adv. Mater.*, 2009, **21**, 2206-2210.
42. X. Wu, G. Q. M. Lu and L. Wang, *Energ. Environ. Sci.*, 2011, **4**, 3565-3572.
43. G. Lee, H. Lee, M.-H. Um and M. Kang, *Bull. Korean Chem. Soc.*, 2012, **33**, 3043-3047.
44. J.-K. Lee, B.-H. Jeong, S.-i. Jang, Y.-G. Kim, Y.-W. Jang, S.-B. Lee and M.-R. Kim, *J. Ind. Eng. Chem.*, 2009, **15**, 724-729.
45. G. Kim, K. Kim, K. Cho and K. Ryu, *Appl. Chem. Eng*, 2011, **22**, 190-195.
46. G. Zhu, L. Pan, J. Yang, X. Liu, H. Sun and Z. Sun, *J. Mater. Chem.*, 2012, **22**, 24326-24329.
47. Y. Li, Z. Che, X. Sun, J. Dou and M. Wei, *Chem. Commun.*, 2014, **50**, 9769-9772.
48. J. Cerda, J. Arbiol, R. Diaz, G. Dezanneau and J. Morante, *Mater. Lett.*, 2002, **56**, 131-136.
49. S. Kanmani and K. Ramachandran, *Renew. Energ.*, 2012, **43**, 149-156.
50. X.-D. Gao, X.-M. Li and X.-Y. Gan, 2013.
51. D. B. Menzies, Q. Dai, L. Bourgeois, R. A. Caruso, Y.-B. Cheng, G. P. Simon and L. Spiccia, *Nanotechnology*, 2007, **18**, 125608.
52. I. G. Yu, Y. J. Kim, H. J. Kim, C. Lee and W. I. Lee, *J. Mater. Chem.*, 2011, **21**, 532-538.
53. I. E. Castelli, D. D. Landis, K. S. Thygesen, S. Dahl, I. Chorkendorff, T. F. Jaramillo and K. W. Jacobsen, *Energ. Environ. Sci.*, 2012, **5**, 9034-9043.
54. W.-Q. Wu, H.-S. Rao, Y.-F. Xu, Y.-F. Wang, C.-Y. Su and D.-B. Kuang, *Sci. Report.*, 2013, **3**.

55.S. Nakade, T. Kanzaki, Y. Wada and S. Yanagida, *Langmuir*, 2005, **21**, 10803-10807.

Figure captions

Fig. 1. (a) Rietveld refinement of the XRD pattern of BSO nanostructures and (b) shows the perovskite structure of BSO

Fig. 2. TEM images of (a-d) BSO, (e) HRTEM image and (f) SAED pattern of synthesized BSO

Fig. 3. Reitveld XRD patterns of the BSO/5 min $TiCl_4$ treatment, BSO/5 min $TiCl_4$ treatment/TiO_2 scattering layer and BSO/5 min $TiCl_4$ treatment/ZnO scattering layer photoelectrodes. (TCL–$TiCl_4$ treatment)

Fig. 4. Surface morphologies of top view of (a) BSO nanostructures, (b) TiO_2 nanoparticles, (f) ZnO nanoparticles. Cross-section view of (c) BSO/TiO_2 scattering layer, (g) BSO/ZnO scattering layer, (d) BSO/1 min $TiCl_4$ treatment/TiO_2 scattering layer, and (h) BSO/1 min $TiCl_4$ treatment/ZnO scattering layer. (e) EDX spectrum of BSO nanostructures

Fig. 5. Schematic diagram of BSO nanostructures based DSCs

Fig. 6. (a, b) show the energy level diagram of the BSO electrode based dye sensitized solar cells. Schematic arrangement of (c) BSO, (d) BSO/$TiCl_4$ treatment, (e) BSO/$TiCl_4$ treatment/TiO_2 scattering layer, and (f) BSO/$TiCl_4$ treatment/ZnO scattering layer.

Fig. 7. Schematic diagram of BSO DSC photoanode with (a) tetragonal TiO_2 nanoparticles and (b) ZnO hexagonal particles scattering layers

Fig. 8. Photocurrent density – voltage curves of DSCs with BSO/$TiCl_4$ treatment/TiO_2 scattering layer photoelectrodes

Fig. 9. Photocurrent density – voltage curves of DSCs with BSO/$TiCl_4$ treatment/ZnO scattering layer photoelectrodes

Fig. 10. Schematic diagram for the photoelectrodes structure with achieved maximum PCE.

Fig. 11. Electron lifetimes as a function of electron density of (a) BSO/$TiCl_4$ treatment/TiO_2 scattering layer electrode and (b) BSO/$TiCl_4$ treatment/ZnO scattering layer electrode.

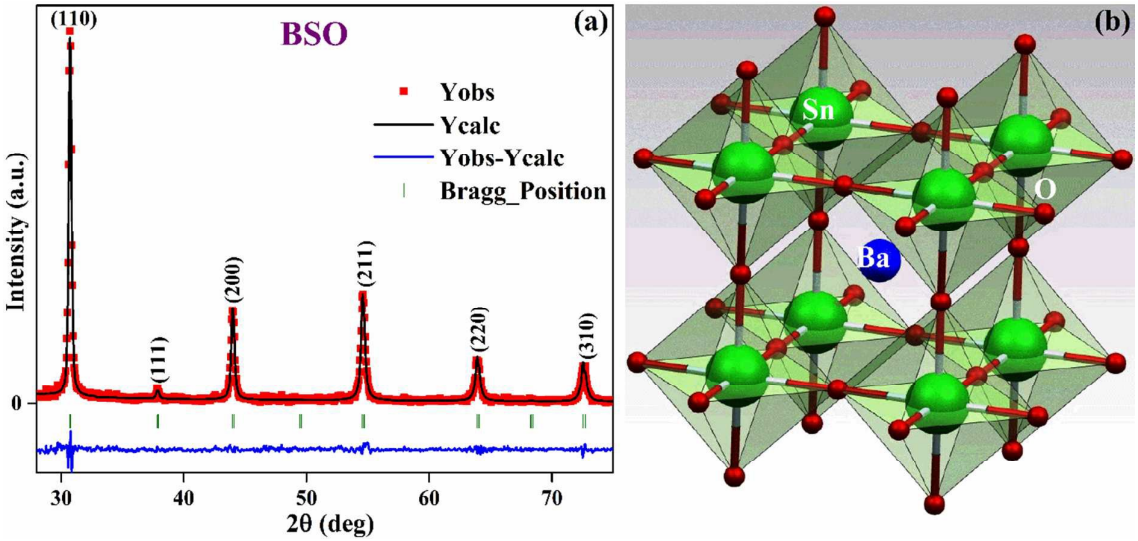

Figure 1

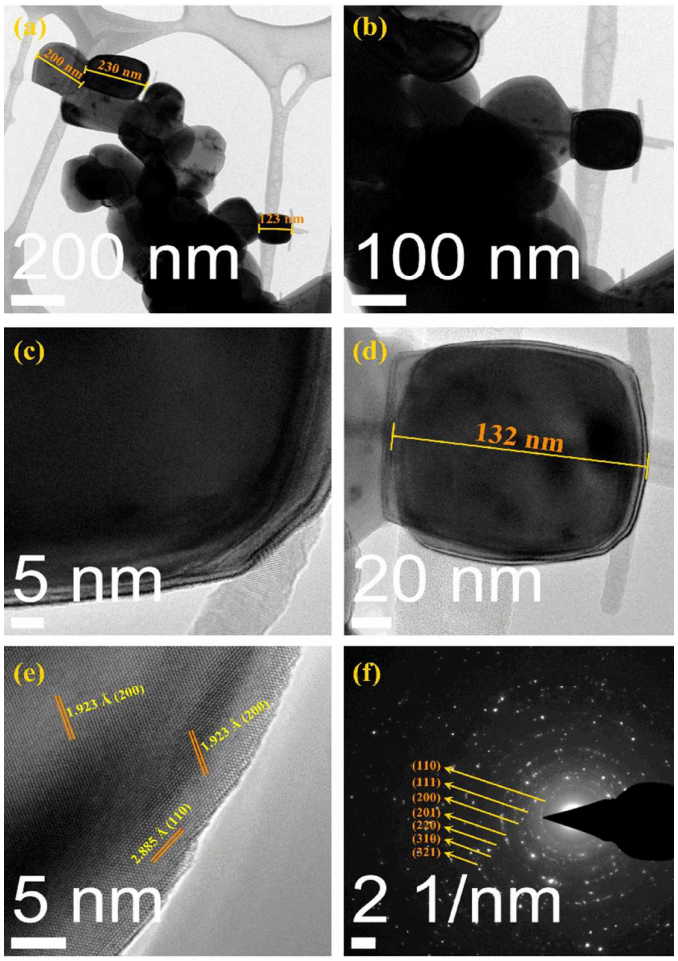

Figure 2

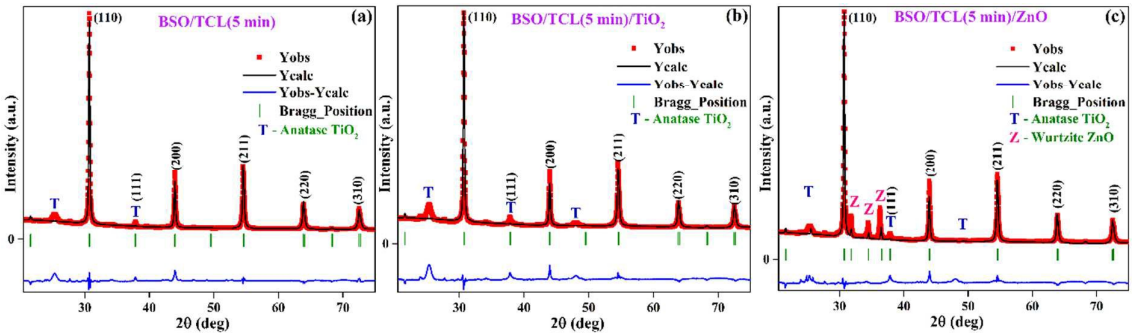

Figure 3

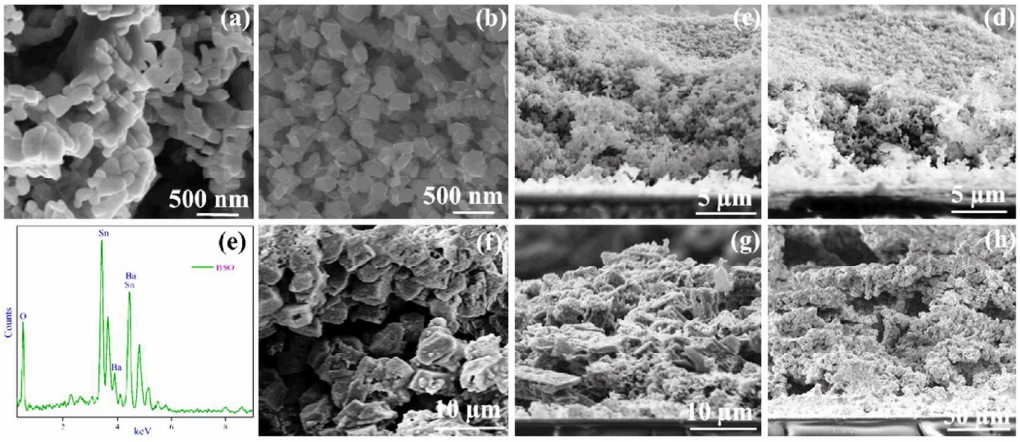

Figure 4

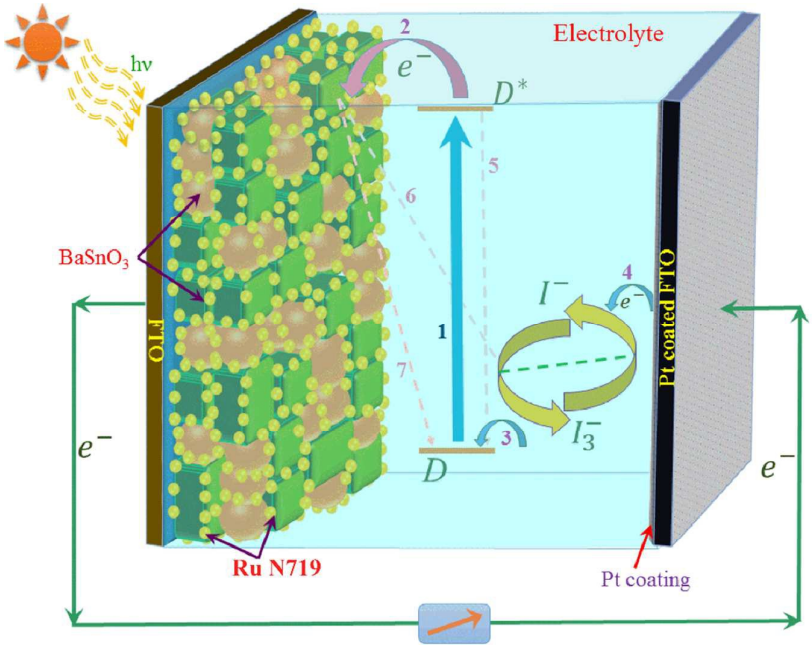

Figure 5

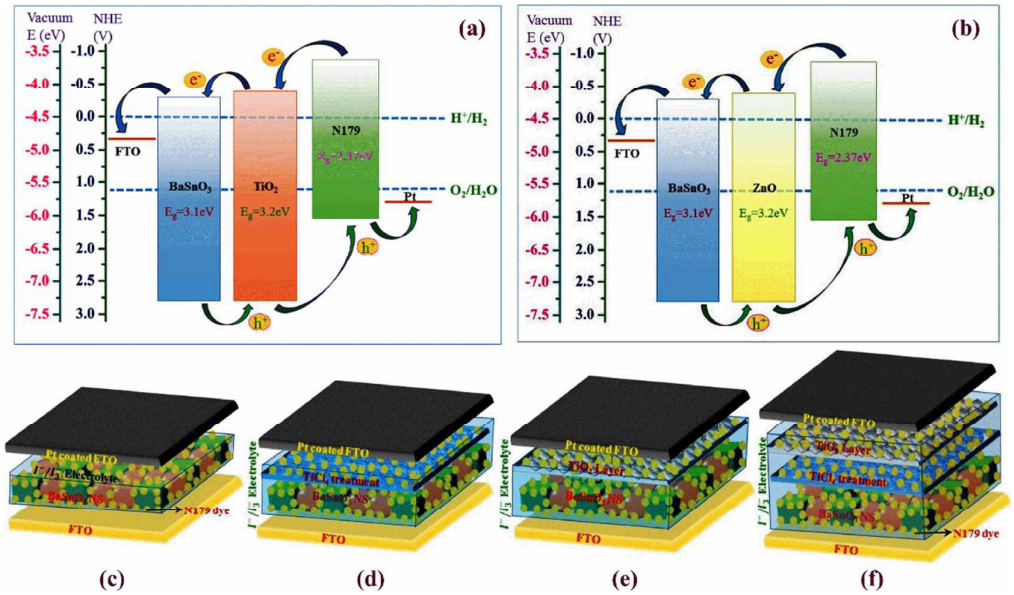

Figure 6

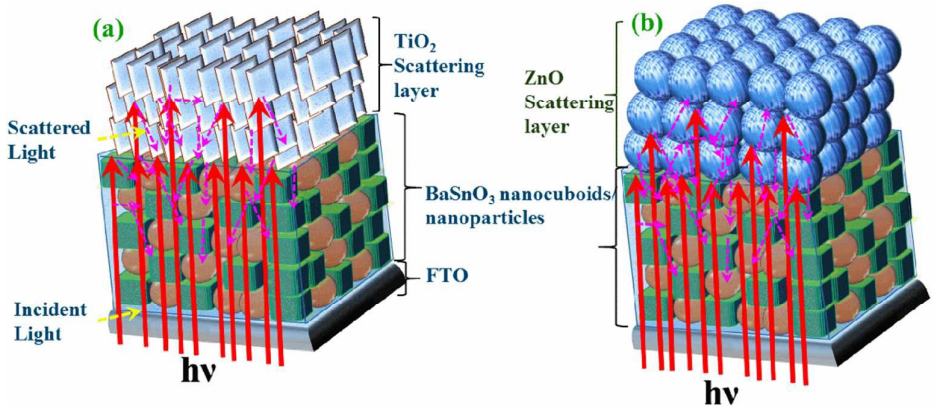

Figure 7

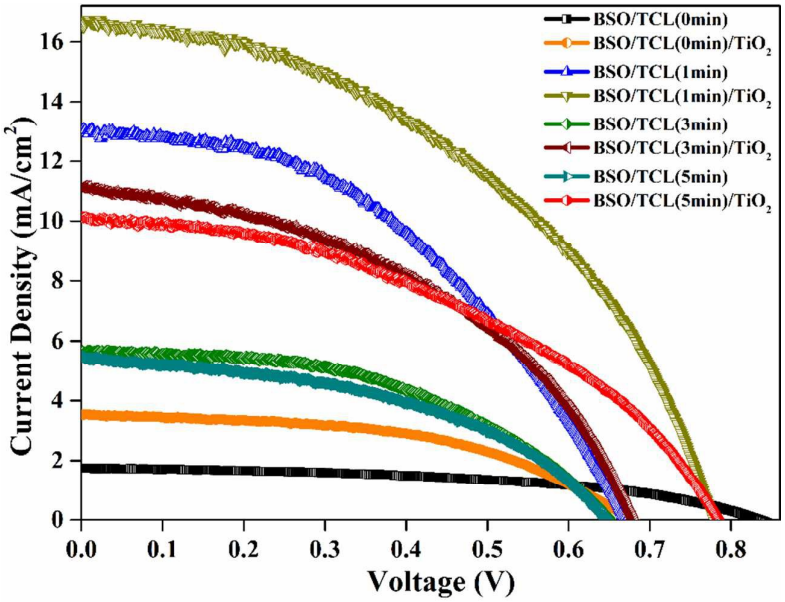

Figure 8

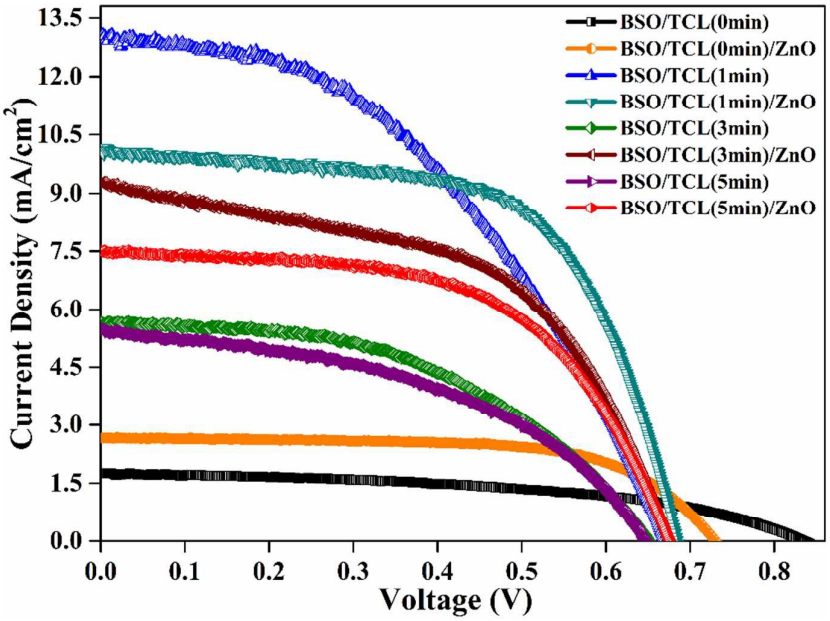

Figure 9

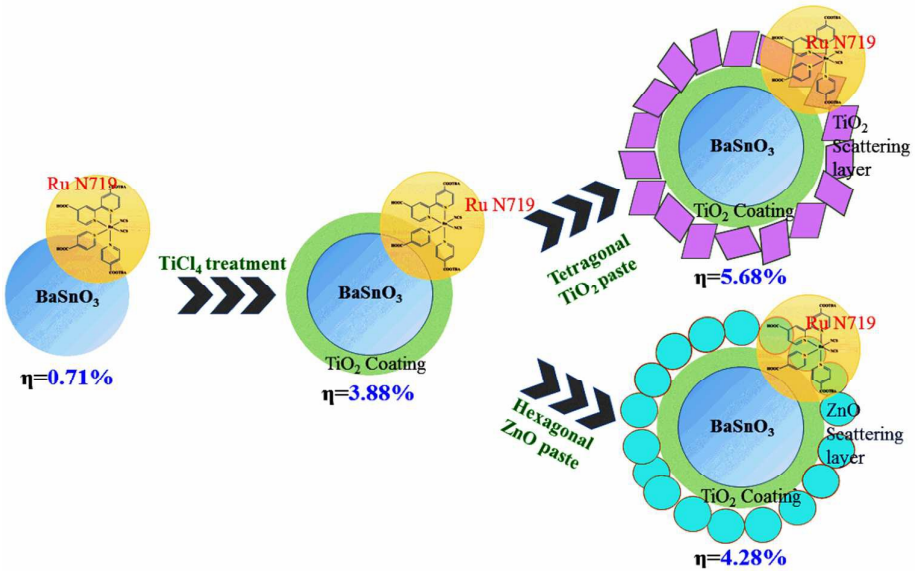

Figure 10

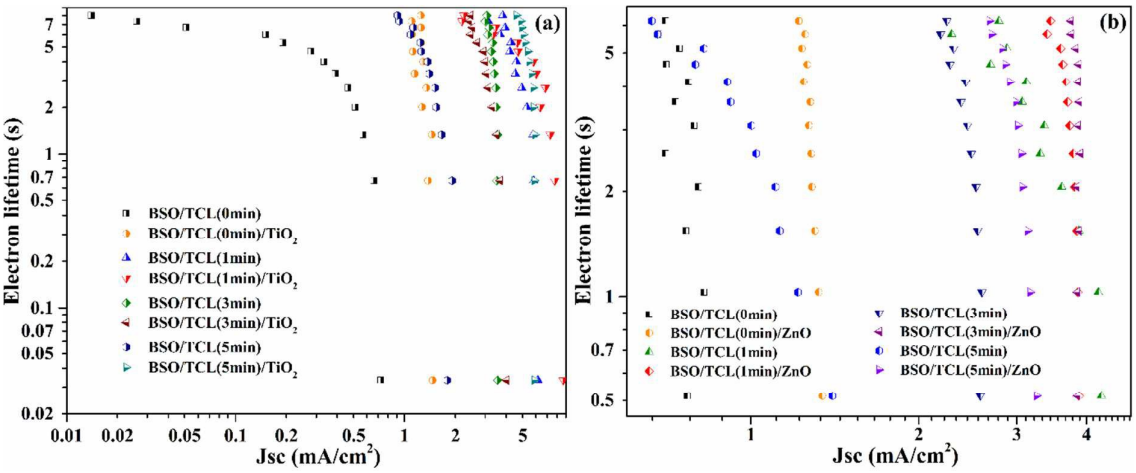

Figure 11

Table 1. XRD results of nanocrystalline cubic perovskite BSO nanostructures

From Rietveld refinement		From XRD calculation	
Volume ($Å^3$)	69.87	Crystallite size D (nm)	23
R-pattern (R_p)	21.5	Lattice parameter (Å)	4.1133(2)
R-weighted pattern (R_{wp})	26.1	Volume ($Å^3$)	69.594
R_{wp} expected (R_{exp})	23.9	Strain (10^{-3})	1.61
R-structure factor (RF)	4.79	Dislocation Density in 10^{15} (lines/m^2)	1.995
Bragg R factor	4.69	JCPDS:15-0780	4.116
S (goodness-of-fit)	1.19	Lattice parameter (Å)	

Here, $R_P = \sum\{y_i(o) - y_i(c)\} / \sum y_i(o)$, $R_{wp} = \sum wi\{y_i(o) - y_i(c)\}^2 / \sum wy_i(o)^2$, $R_{\exp} = \{(N-P) / \sum w_i y_i(o)^2\}^{1/2}$, $S = R_{wp} / R_{\exp} y_i(o)$ and $y_i(c)$ are observed and calculated intensities at profile point i, respectively & w_i is the weight for each Step i. N and P are number of experimental observations and the number of fitting parameters.

Table 2. Photocurrent density-voltage characteristics of $BaSnO_3$ based DSCs with different $TiCl_4$ treatment times and TiO_2 and ZnO scattering layer.

BSO condition	J_{sc} (mA cm^{-2})	V_{oc} (V)	Fill factor	Efficiency η (%)
BSO/TCL (0 min)	1.744	0.837	0.49	0.71
BSO/TCL (0 min)/TiO_2	3.569	0.667	0.48	1.14
BSO/TCL (0 min)/ZnO	2.660	0.734	0.64	1.25
BSO/TCL (1 min)	13.082	0.667	0.45	3.88
BSO/TCL (1 min)/TiO_2	16.677	0.776	0.44	5.68
BSO/TCL (1 min)/ZnO	10.020	0.686	0.62	4.28
BSO/TCL (3 min)	5.677	0.651	0.48	1.78
BSO/TCL (3 min)/TiO_2	11.133	0.677	0.44	3.32
BSO/TCL (3 min)/ZnO	9.304	0.676	0.52	3.25
BSO/TCL (5 min)	5.484	0.648	0.45	1.61
BSO/TCL (5 min)/TiO_2	10.130	0.784	0.41	3.27
BSO/TCL (3 min)/ZnO	7.535	0.676	0.56	2.87

TiO_2 – TiO_2 scattering layer; ZnO – ZnO scattering layer; TCL – $TiCl_4$ treatment